Supporting Information

Novel Green Fabrication of Stable Hydrogel Beads from Industrial Waste Lignin for Efficient Pb(II) Ion Removal

Xiwen Hu[ab], Muhammad Amirul Islam[*ab], Aria Khalili[ab], Amir Aghaei[ab], Jae-Young Cho[b], Mohtada Sadrzadeh[*a]

[a] Department of Mechanical Engineering, 10-367 Donadeo Innovation Center for Engineering, Advanced Water Research Lab (AWRL), University of Alberta, Edmonton, AB, T6G 1H9, Canada

[b] Quantum and Nanotechnologies Research Centre, National Research Council Canada, 11421 Saskatchewan Drive, Edmonton, AB, T6G 2M9, Canada

[*]Corresponding authors:

Mohtada Sadrzadeh (sadrzade@ualberta.ca)

Mohammad Amirul Islam (maislam@ualberta.ca, Muhammad.Islam@nrc-cnrc.gc.ca)

S1. Method of fabricating SKLGE beads

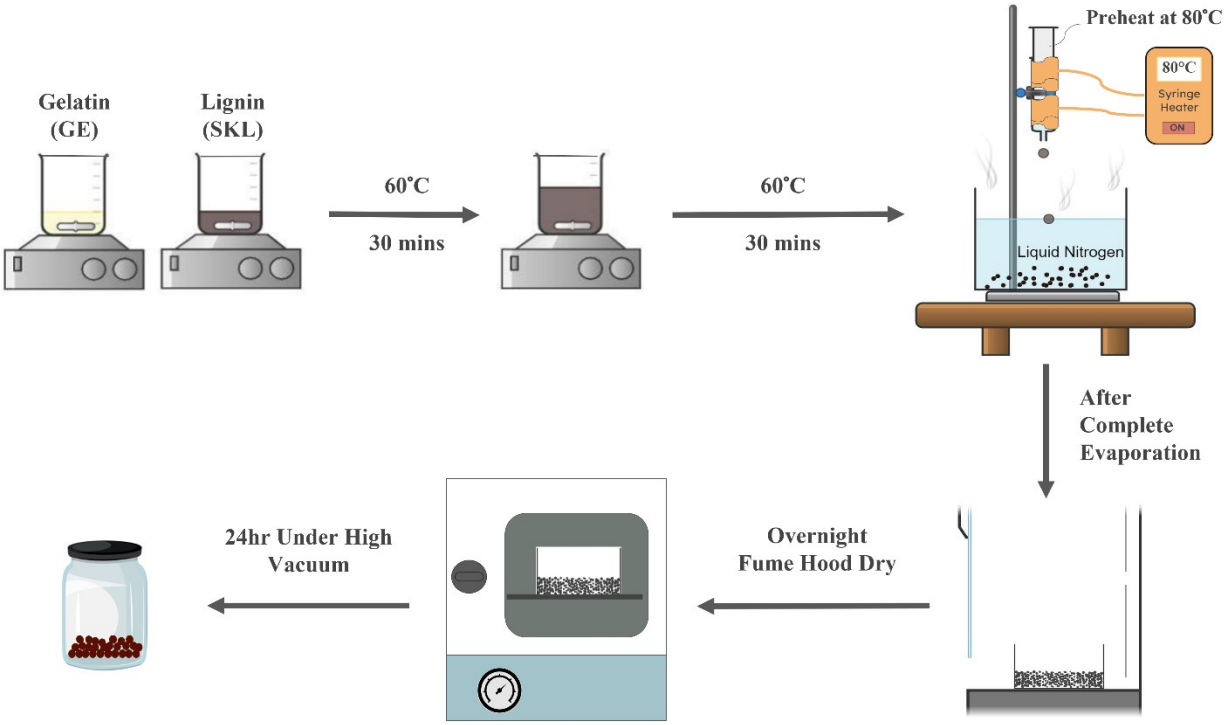

Fig S1. Schematic of the fabrication process of SKLGE beads

Table S1. Lignin and gelatin weight ratios in SKLGE beads

Name	Lignin (wt%) vs Gelatin (wt%)		Total concentration (wt%)	MilliQ Water Volume (mL)
GE10	0	10	10	18
SKL25	25	75	10	18
SKL30	30	70	10	18
SKL35	35	65	10	18
SKL40	40	60	10	18
SKL45	45	55	10	18
SKL50	50	50	10	18
SKL45-7.5wt%	45	55	7.5	18
SKL45-12.5wt%	45	55	12.5	18

Table S2. EDC/NHS solution preparation for cross-coupling 0.05g dry beads

EDC Concentration (mM)	EDC.HCl (mg)	NHS (mg)	DIPEA (uL)	MilliQ water (mL)
0.5	0.96	0.59	0.88	10
1	1.92	1.17	1.75	10
2	3.84	2.34	3.5	10
4	7.67	3.5	7	10

Table S3. Composition of UV-Vis test solutions

MilliQ water (mL)	Borate Buffer (mL)	PAR Volume (mL)	Sample solution volume (mL)	Total Test Solution Volume (mL)
23.1	0.6	1	0.3	25
22.9	0.6	1	0.5	25
22.4	0.6	1	1	25
21.4	0.6	1	2	25

Table S4. Methodologies applied for fabrication of SKLGE beads

Dispersion medium	Solution Temperature	Gelation medium	Cooling Temperature	Fabrication speed	Pros or cons
Water	60 °C	Water	23 °C	Slow	Film floating on water
Water	60 °C	Mineral Oil	23 °C	Slow	Droplets coalesce
DMSO	60 °C	Methanol	23 °C	Slow	Film on methanol
Water	60 °C	Kerosene	23 °C	Slow	Droplets coalesce
Water	60 °C	Kerosene	-20 °C	Medium	Kerosene waste and slow speed
Water	60 °C	Liquid Nitrogen	-196 °C	Rapid	Most effective; porous interior and dense skin

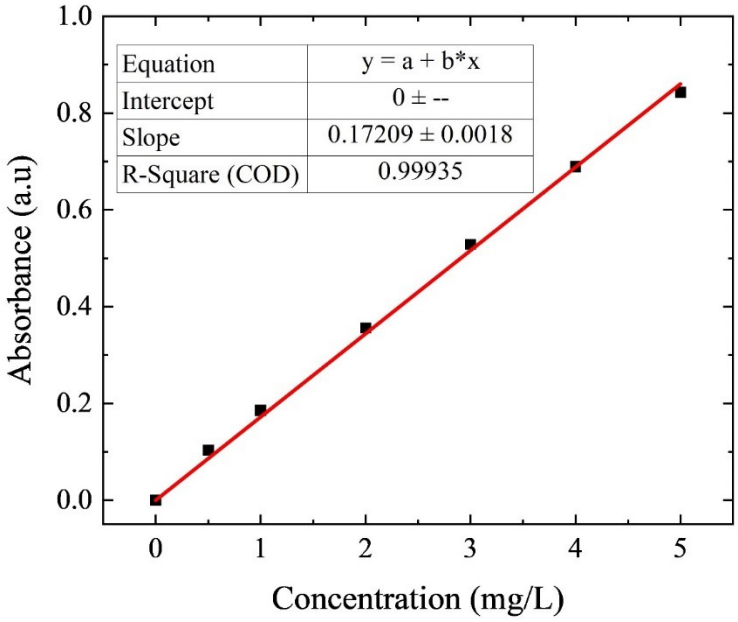

Fig S2. Calibration curve for UV-VIS method for the determination of the Pb(II) ion concentration.

S2. Adsorption and desorption experiments

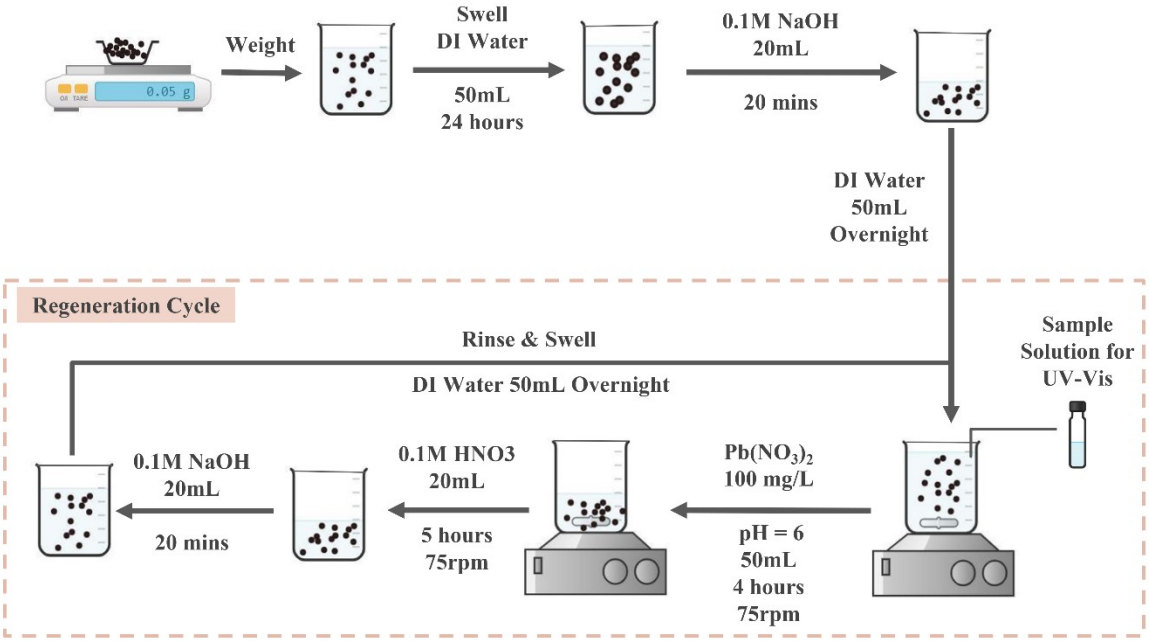

Fig S3. Schematic representation of the adsorption and desorption cycle experiments.

S3. Effect of pH on adsorption

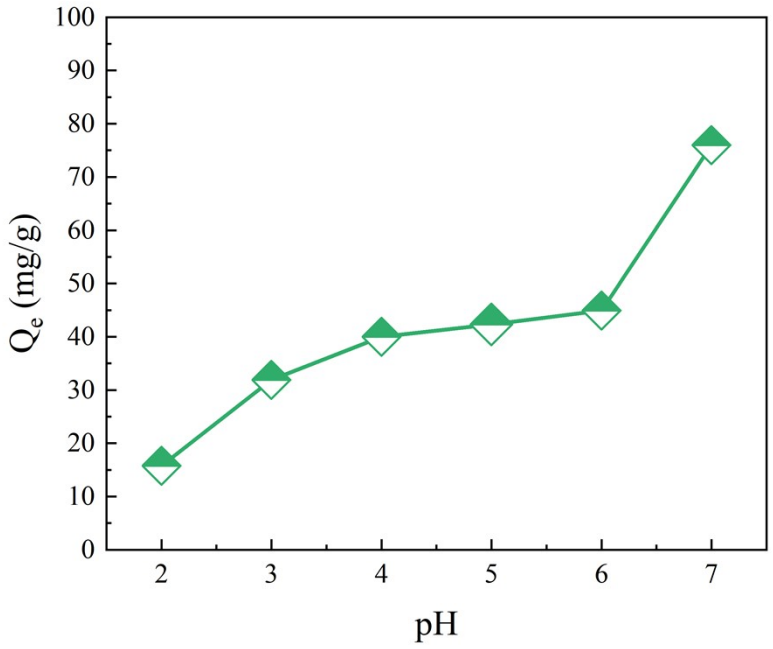

Fig S4. Effect of pH on the adsorption capacity (Q_e) of SKL45 for Pb(II) ions.

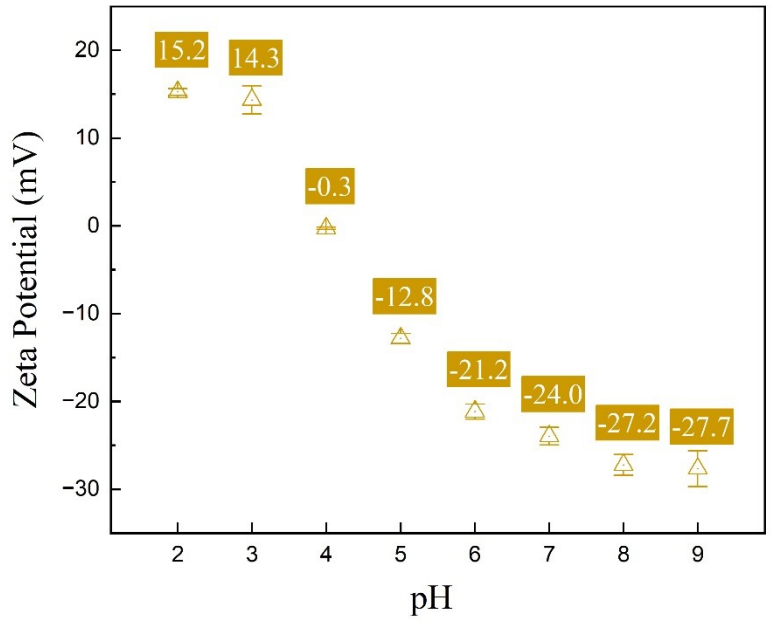

Fig S5. Variation in zeta potential with pH for the gelator solution, containing 45% SKL and 55% gelatin, corresponding to the ratio in SKL45 beads.

S4. Examining bead pretreatment and regeneration process

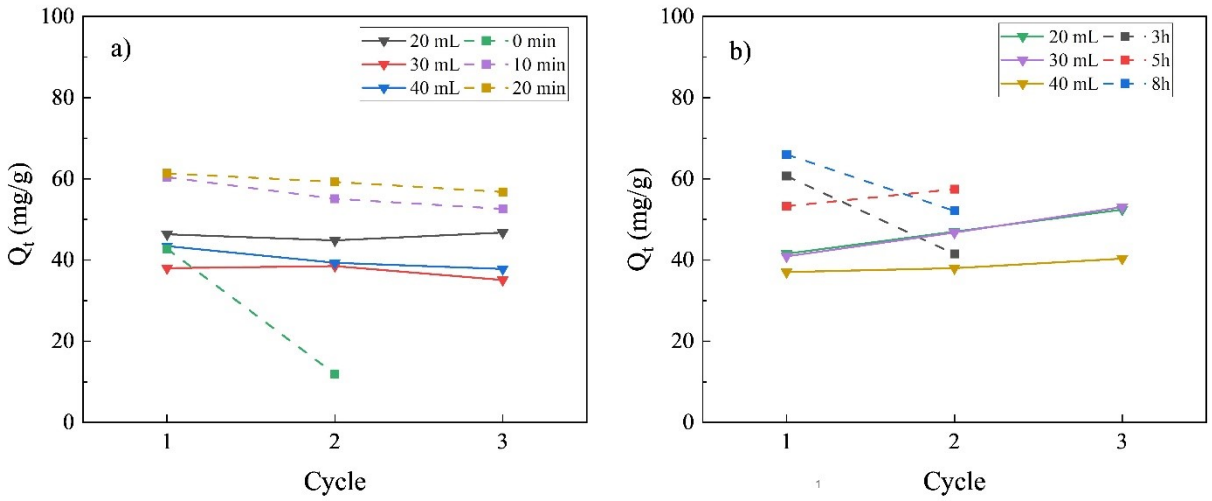

Fig S6. Effect of (a) NaOH and (b) HNO_3 volume and contact time on adsorption and desorption processes.

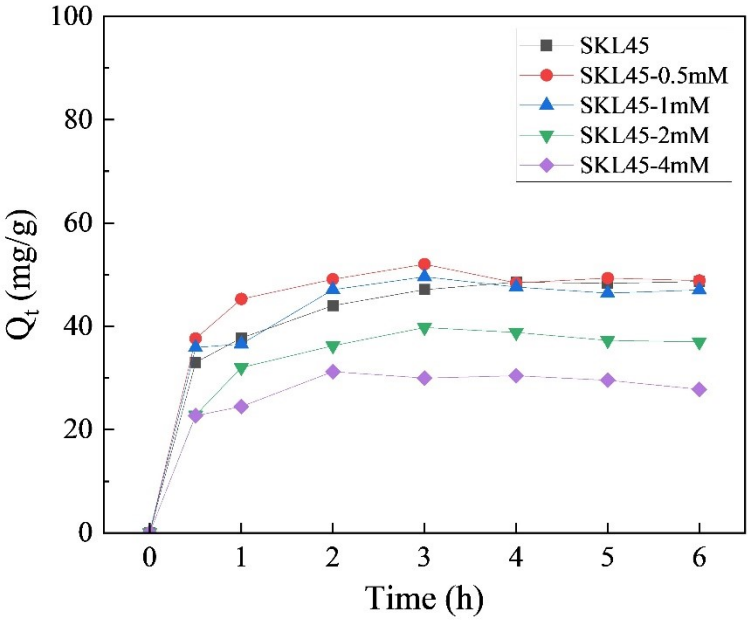

S5. Identifying the adsorption kinetics

Fig S7. Effect of contact time on the adsorption capacity of 0, 0.5, 1. 2, and 4 mM EDC cross-coupled SKL45 beads. Experiments were conducted at an initial concentration (C_0) of 100 mg/L, with a bead dosage of 0.05 g per 50 mL, at pH 6, and a stirring rate of 75 rpm.

S6. Optimization of bead composition

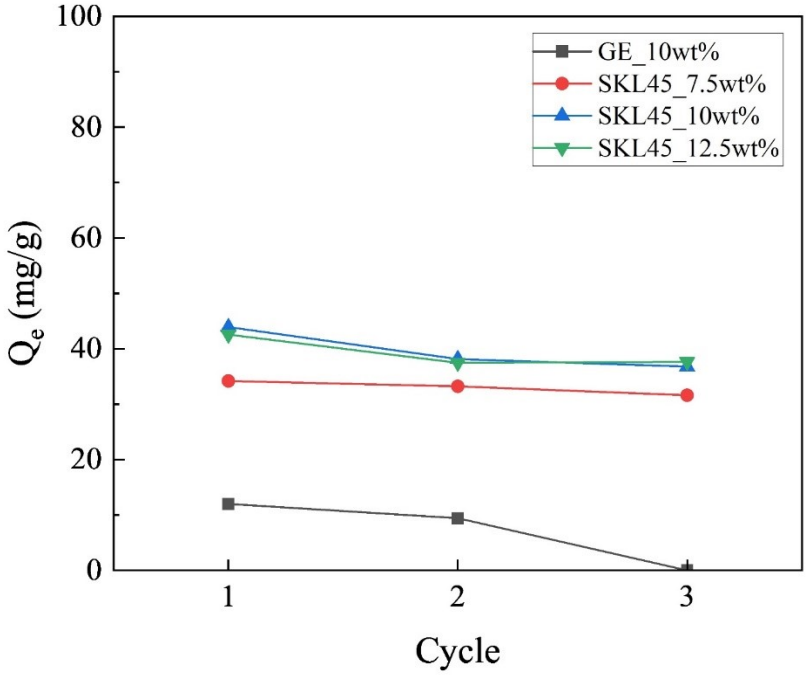

Fig S8. Effect of SKL weight percentage on the stability of beads over multiple adsorption-regeneration cycles

S7. Effect of adsorbent dosage on Pb(II) ion adsorption

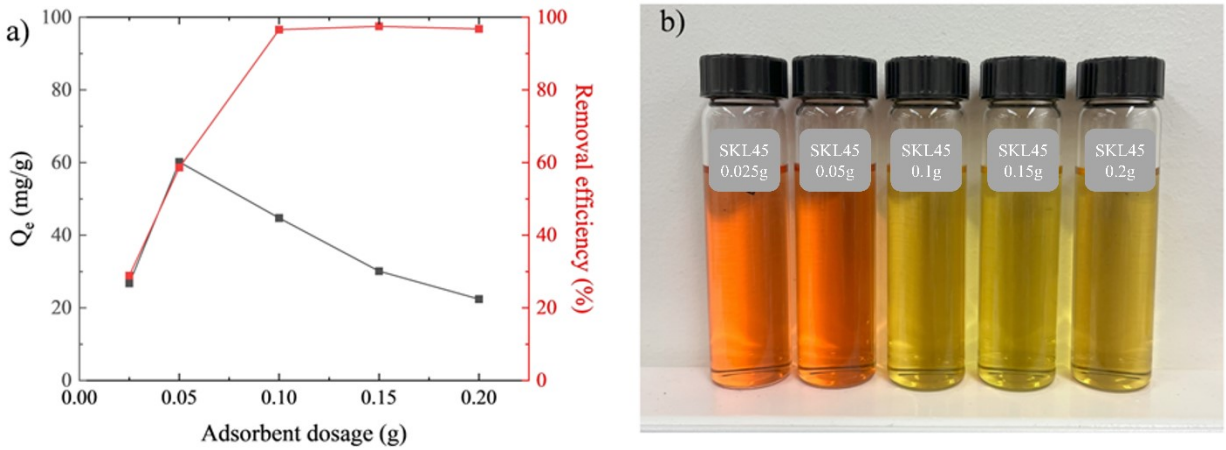

Fig S9. Effects of SKL45 adsorbent dosage on Pb(II) ion adsorption: (a) Plots of adsorption capacity and removal efficiency as a function of SKL45 dosage, (b) Photographs illustrating the near-complete removal of Pb(II) ions by 0.1 g beads and above, evidenced by the absence of color in the Pb-PAR complex. C_0: 100 mg/L, volume: 50 mL, pH: 6.0, time: 4h, stirring rate: 75 rpm.

S8. Effect of Pb(II) ion initial concentration on adsorption

Table S5. Comparison of Pb(II) ion adsorption capacity of SKL45 beads with other lignin-based spherical adsorbents.

Type of adsorbent	Crosslinkers used/gelation process	Parameters	Experimental Adsorption capacity (mg/g)	Regeneration	Ref
Ca-alginate-lignin beads	$CaCl_2$ crosslinking	100 mg/L, pH 5, 8 h, 37 ℃	77.22	Five cycles; 1 M HNO_3	40
Lignin-sodium alginate beads	$CaCl_2$ crosslinking	0.4g, 210 mg/L, 25 °C, 40 °C, 55 °C, pH 5, 2h	191.0, 260.7, and 365.4 at 25, 40, and 55 °C, respectively	Five cycles; 0.01 M HNO_3	36
Lignin-PEI microspheres	Chemical crosslinking by epoxy chloropropane	0.1 g, 50 mL 120 mg/L, 3h, pH 6, 25 °C, 35 °C, 45 °C	33.9, 36.1, and 37.3 mg/g at 25, 35, 45 °C, respectively.	Five cycles; 0.1 M HNO_3 and 0.1 M NaOH	39
Carboxymethyl lignin nanospheres	Self-assembly by π–π interactions	0.3g, 50 mL 100 mg/L, 3h, 30 °C, pH 6.03	333.26	Ten cycles; 0.1 M HNO_3 and 0.1 M NaOH	26
Lignin derivate magnetic hydrogel microspheres	DETA-lignin-Fe_3O_4-complex	10 mg, 20 mL Pb (conc not reported), pH 5, 25 °C, 24h	33	Three cycles; 5mL DI water	41
Porous polyamine lignin microsphere	Chemical crosslinking by epoxy chloropropane	0.1 g, 50 mL 500 mg/L, 30 °C, 4h, pH 5	156.82	Five cycles; 0.1 M HNO_3	38
Crosslinked porous lignin beads	Chemical crosslinking by epichlorohydrin	100 mg, 50 mL 240mg/L, pH 6.5, 12 h, 25 ℃	44.5	One cycle; 3 M HCl	42
Dual-modified lignin-sodium alginate assembled multilayer microsphere	$CaCl_2$ crosslinking	40 mg dosage, 50 mL 30 mg/L Pb, pH 5, 3h,30 °C	187.5	Three cycles; 1M HCl	37
Carboxymethalated and	Cooling and	0.04 g, 100 mL	26.9	Not reported.	43

Fe_3O_4 magnetized lignocellulosic hydrogel beads	coagulation from water by self-assembly	20 mg/L Pb, pH 5.3, 25 °C, 24h			
Sulphonated kraft lignin-gelatin beads	Cooling in Liquid Nitrogen, self-assembly	0.05g SKL45, 50 mL 1000 mg/L Pb, pH 6; 23 °C, 4h	155	Ten cycles; 0.1M HNO_3, 0.1M NaOH	This study

S9. Langmuir and Freundlich isotherm models

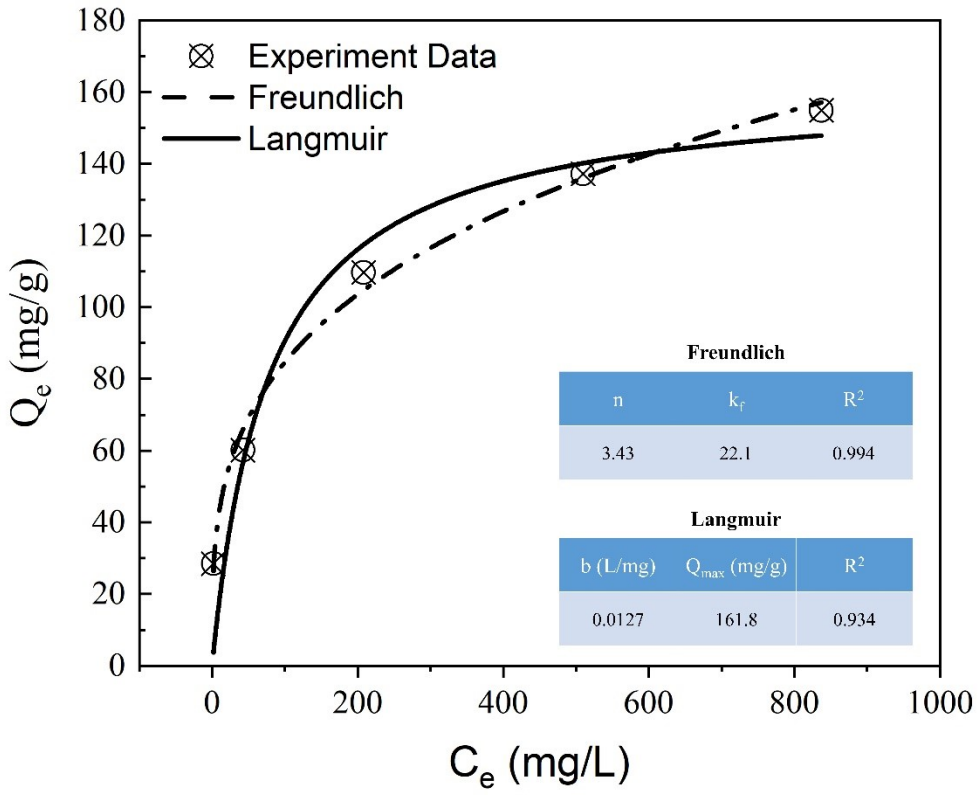

Fig S10. Langmuir and Freundlich adsorption isotherm nonlinear models for SKL45 bead's Pb(II) ion adsorption.

S10. XPS evaluation of the Pb(II) adsorption process on SKL45

XPS can be utilized to determine whether Pb(II) ion adsorption is chemisorption, as this process should result in different chemical environments for the elements to which Pb(II) ions are adsorbed, leading to shifts in the binding energy of the corresponding peaks. As presented in **Fig 5a,** the elemental composition of SKL45 calculated from survey XPS is 64.76% for C, 22.60% for O, 8.99% for N, 2.20% for S, and 1.46% for Na. Note that the S atoms originate from the $–SO_3^-$ groups on SKL, while Na comes from the counterions associated with all NaOH-ionized functional groups on both SKL and GE. After Pb(II) adsorption, the elemental composition is 60.88% for C, 25.81% for O, 9.16% for N, 2.36% for S, and 1.79% for Pb. The complete replacement of Na from the ionized -COOH, $-SO_3H$, and Ph-OH functional groups by Pb indicates that Pb was chemisorbed onto these functional groups by forming coordination complexes.

Chemisorption is also supported by the shift in the binding energy of Pb $4f_{7/2}$ and Pb $4f_{5/2}$ from 139.5 eV and 144.4 eV for $Pb(NO_3)_2$ to 139.1 eV and 143.9 eV (**Fig 5b**) [1]. The C1s peak was deconvoluted into three distinct regions corresponding to carbon atoms in different chemical environments, labeled as C1, C2, and C3 (**Fig 5c**, **d**). The SKL45 sample exhibits a C1 peak at 284.8 eV, indicating C–C and C=C bonds in both aliphatic and aromatic hydrocarbons. Additionally, the C–O peak from carboxylate ($O=C–O^-$) and phenoxide ($Ph–O^-$) ions may shift to lower binding energy due to the extra electron density from the negative charge on the oxygen, merging with the peaks for C–C and C=C and contributing to the peak area for C1. The C2 peak, centered at 286.0 eV, corresponds to C–N, C–O, and C=O functionalities from amides, carboxylic acids, phenols, alcohols, ethers, and aldehydes. Lastly, the C3 peak, observed at 288.0 eV, is attributed to C=O bonds from amides and carboxylic acids. The most notable observation in the XPS evaluation following Pb(II) ion adsorption is the reduction of the peak area of C1 for C–C and C=C bonds to 1.4 times, alongside an increase in the peak area for C–O and C–N bonds to 1.3

times that in SKL45 (**Fig 5c, d** and **Table 2**). The reduction in C–C and C=C peak area can be attributed to the shift of the C=C band to higher binding energy due to M-π interactions, contributing to the increased peak area for C–N and C–O bonds (**Table 2**). A different interpretation of the observed peak shift and area change is that in SKL45, the phenoxide group carries a negatively charged oxygen atom, which participates in resonance stabilization with the aromatic rings. This additional electron density on the aromatic rings contributes to a lower binding energy for the C=C bonds. However, when Pb(II) ions form a coordination complex with the phenoxide groups, the negative charge on the oxygen becomes unavailable for resonance stabilization, and electron density is withdrawn from the aromatic rings. This shift results in the C=C bond peak moving to a higher binding energy and merging with the C–O bond peak, leading to a decrease in the C1 peak area and an increase in the C2 peak area. A third explanation could be that the complexation of carboxylate and phenoxide $C–O^-$ ions with Pb(II) ions removes the negative electron charge from these ions. Consequently, the peaks that originally merged with the C1 peak for C–C and C=C bonds shift back to their original positions for non-ionized carboxylic acids and phenolic C–O bonds, increasing the peak area for the C2 peak. The involvement of any of these three processes supports the chemisorption of Pb(II) ions onto the ionic functional groups present in both SKL and GE, with the binding of SKL predominating.

The second notable observation from the XPS analysis is the stark contrast in the O1s region (**Fig 5e, f**). The O1s spectrum was deconvoluted into two regions: the O1 region at 531.4 eV represents C=O and S=O bonds from aldehydes, carboxylic acids, amides, and sulfonic groups, as well as C–O and S–O bonds from ionic carboxylate, phenoxide, and sulfonate groups. In contrast, the O2 region at 532.7 eV corresponds to C–O and S–O bonds from alcohols, ethers, and non-ionized phenolic, carboxylic, and sulfonic groups [41, 42, 43]. The area ratio of the O2 region to the O1

region was more than double in SKL45 after Pb(II) ion adsorption compared to before (**Table 2**). This increase in the O_2 region may be attributed to the shift of the peaks for C–O and S–O bonds from ionized carboxylate, phenoxide, and sulfonate groups due to complexation with Pb(II) ions, which removes the negative electron charges from oxygen. This further suggests the chemisorption of Pb(II) ions onto the SKL45 beads.

S11. Zero-length EDC cross-coupling to enhance bead stability

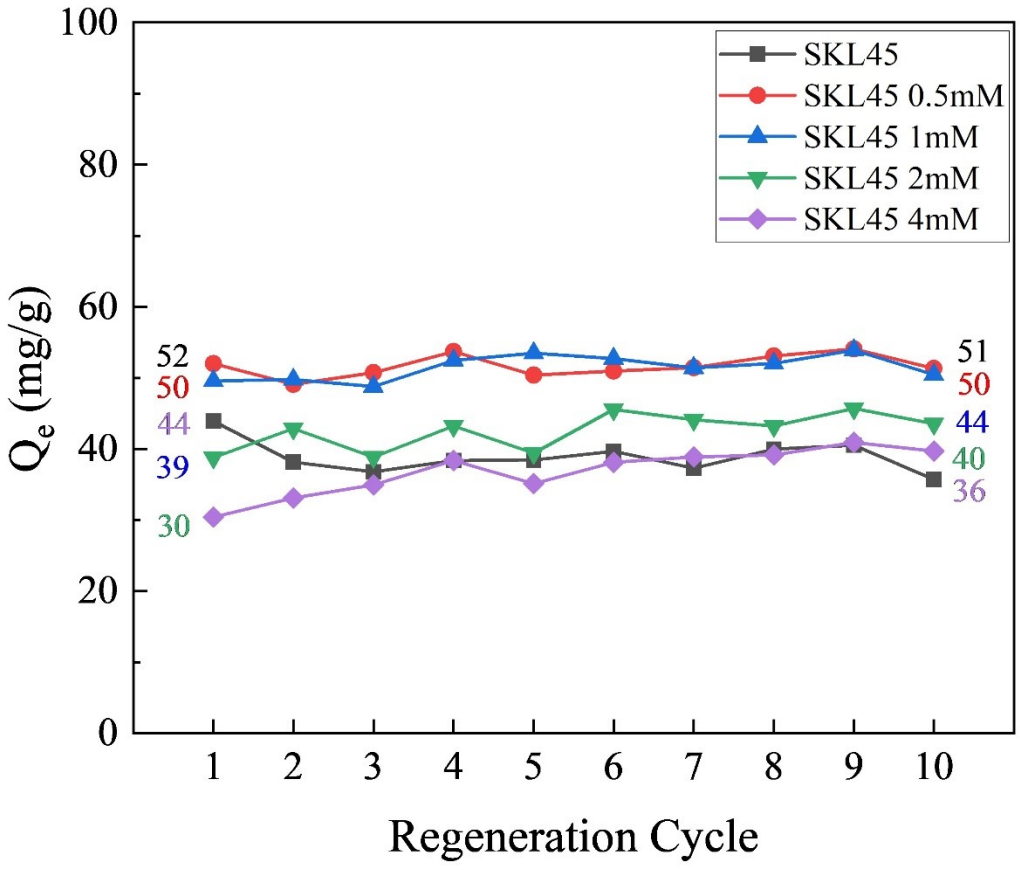

Fig S11. Adsorption result for EDC cross-coupled SKL45 for ten continuous regeneration cycles. Experiments were conducted at an initial concentration (C_0) of 100 mg/L, with a bead dosage of 0.05 g per 50 mL, at pH 6, and a stirring rate of 75 rpm.

S12. Thermal stability of gel in EDC-crosslinked and non-crosslinked SKL45 beads

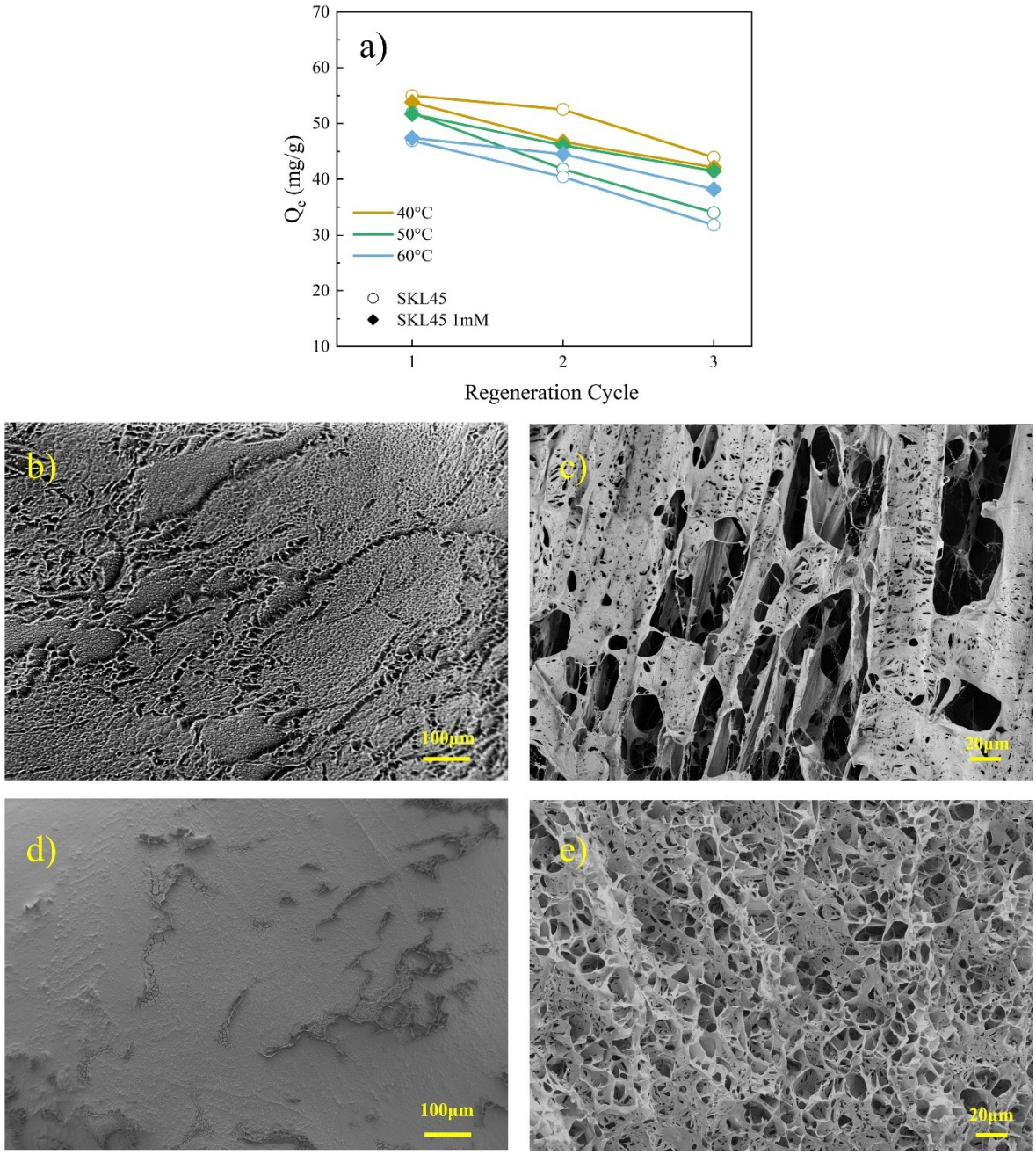

Fig. S12. Effect of temperature the adsorption capacity and gel morphology: (a) Adsorption results for SKL45 and EDC 1mM cross-coupled SKL45 over three regeneration cycles. Experiments were performed with an initial concentration (C_0) of 100 mg/L, a bead dosage of 0.05 g per 50 mL, at pH 6, and temperatures of 40°C, 50°C, and 60°C, with a stirring rate of 75 rpm. Cryo-SEM images display the shell and cross-sectional interior of SKL45 beads (b, c) and SKL45 1mM beads (d, e) after three adsorption-regeneration cycles at an adsorption temperature of 60°C.